

## Induction of Flexibility through Protein-Protein Interactions\*

Received for publication, January 27, 2003, and in revised form, February 20, 2003  
Published, JBC Papers in Press, February 25, 2003, DOI 10.1074/jbc.M300866200

Rosa Fayos‡, Giuseppe Melacini‡, Marceen G. Newlon‡, Lora Burns‡, John D. Scott§¶, and Patricia A. Jennings‡¶||

From the ‡Department of Chemistry and Biochemistry, University of California, San Diego, La Jolla, California 92093-0359 and the §Howard Hughes Medical Institute, Vollum Institute, Portland, Oregon 97201

**The dimerization/docking (D/D) domain of the cyclic AMP-dependent protein kinase (PKA) holoenzyme mediates important protein-protein interactions that direct the subcellular localization of the enzyme. A kinase anchoring proteins (AKAPs) provide the molecular scaffold for the localization of PKA. The recent solution structures of two D/D AKAP complexes revealed that the AKAP binds to a surface-exposed, hydrophobic groove on the D/D. In the present study, we present an analysis of the changes in hydrogen/deuterium exchange protection and internal motions of the backbone of the D/D when free and bound to the prototype anchoring protein, Ht31<sub>pep</sub>. We observe that formation of the complex results in significant, but small, increases in H/D exchange protection factors as well as increases in backbone flexibility, throughout the D/D, and in particular, in the hydrophobic binding groove. This unusual observation of increased backbone flexibility and marginal H/D exchange protection, despite high affinity protein-ligand interactions, may be a general effect observed for the stabilization of hydrophobic ligand/hydrophobic pocket interactions.**

Protein-protein interactions control many critical functions in biology, ranging from tight binding antibody-antigen recognition events to transient interactions between enzymes in a signaling pathway. These interactions can be complex; there are sometimes a number of diverse proteins that can interact with a particular target molecule (1, 2). Elucidation of key intermolecular contacts between protein partners can aid in the development of small molecule inhibitors and/or promoters of these important interactions, which in turn control function. A particularly interesting area in biology today is the investigation of the molecular mechanisms of the assembly/disassembly of signaling networks in response to a specific cellular signal (3). Indeed, the spatio-temporal compartmentalization of signaling molecules affords biological control by poising interacting partners in close proximity to substrate(s) and/or regulatory elements (4).

Targeting of the cyclic AMP-dependent protein kinase (PKA)<sup>1</sup> holoenzyme through interactions with A kinase anchor-

ing proteins (AKAPs) has emerged as an important modulator of PKA activity in diverse tissues (5). The PKA holoenzyme consists of a regulatory subunit (R<sub>2</sub>) dimer and two catalytic (C) subunits (6). Phosphorylation of target proteins is carried out by the C subunit, whereas the N-terminal 45 residues of the R subunit mediates both dimerization and subcellular localization via AKAP recognition (7, 8). Hence, the N-terminal functional domain is termed a D/D motif because it dimerizes and docks to anchoring partners. Solution structural studies revealed that the type II $\alpha$  D/D of PKA packs into an antiparallel, dimeric X-type four-helix bundle, with a surface-exposed hydrophobic groove that is the site of anchoring interactions (9, 10).

PKA interacts with a diverse family of proteins. Sequence alignment of the identified AKAPs, to date, reveals no specific recognition sequence for the D/D. However, a conserved structure consistent with an amphipathic helix was predicted, and has been demonstrated in recent solution structural studies of a peptide derivative of the prototypic AKAP human thyroid anchoring protein Ht31 (residues 493–515 and designated Ht31<sub>pep</sub>) (7, 11, 12). This peptide derivative of Ht31 exhibits a nanomolar binding affinity for the type II D/D (12, 13) via hydrophobic-hydrophobic interactions between the surface-accessible hydrophobic groove on the D/D and the hydrophobic face of the AKAP-derived amphipathic helix (10, 14).

In an effort to gain a better understanding of the physicochemical basis for PKA-AKAP interactions, we initiated hydrogen/deuterium (H/D) exchange and backbone relaxation studies of the D/D free and in complex with Ht31<sub>pep</sub>. In contrast to recent work described by Powell *et al.* (15) using H/D exchange to measure ligand-binding affinities, we observe only modest changes in the H/D protection factors upon complex formation, despite the nanomolar binding affinity of Ht31 for the D/D (11). Unexpectedly, we also find that backbone flexibility in the binding interface of the D/D increases in the Ht31<sub>pep</sub> complex. We propose that the increase in backbone mobility and display of modest changes in H/D exchange protection factors upon high affinity ligand binding may be a general effect observed for proteins that use solvent accessible hydrophobic surfaces to recognize diverse binding partners.

### EXPERIMENTAL PROCEDURES

**Sample Preparation**—The D/D-Ht31<sub>pep</sub> peptide complex was prepared as described previously (16). The Ht31<sub>pep</sub> peptide was obtained from PeptidoGenic Research and Co. (Livermore, CA). The stoichiometry of binding for classical AKAPs is one AKAP per R subunit dimer (11). The apo-D/D was prepared as a 0.25 mM (0.5 mM monomer) sample in 20 mM sodium phosphate buffer, 90% H<sub>2</sub>O, 10% D<sub>2</sub>O, pH 4.0. Relaxation experiments were collected on either a 0.25 mM (0.50 mM monomer apo) or a 0.50 mM (1.0 mM monomer complex) sample. Samples for hydrogen/deuterium exchange studies were collected on 0.25–1.0 mM protein solutions.

**Hydrogen/Deuterium Exchange Studies**—Hydrogen/deuterium exchange experiments were initiated by introducing the protein samples

\* This work was supported in part by grants from NATO, the LJIS (La Jolla Interface in Science) Interdisciplinary Training Program, and The Burroughs Wellcome Fund. The costs of publication of this article were defrayed in part by the payment of page charges. This article must therefore be hereby marked "advertisement" in accordance with 18 U.S.C. Section 1734 solely to indicate this fact.

¶ Supported by National Institutes of Health Grant DK54441.

|| To whom correspondence should be addressed: Dept. of Chemistry and Biochemistry, University of California, San Diego, 9500 Gilman Dr., La Jolla, CA 92093-0359. Tel.: 858-534-6417; Fax: 858-534-7042; E-mail: pajennin@chem.ucsd.edu.

<sup>1</sup> The abbreviations used are: PKA, cyclic AMP-dependent protein kinase; AKAP, A kinase anchoring protein; D/D, dimerization/docking.

TABLE I  
Hydrogen/deuterium exchange parameters

Residue	Intrinsic Rate (sec <sup>-1</sup> )	APO Rate (sec <sup>-1</sup> )	APO Protect. Factor	APO ΔG (Kcal/mol)	COMPLEX Rate (sec <sup>-1</sup> )	COMPLEX Protect. Factor	COMPLEX ΔG (Kcal/mol)
met0	0.018		1			1	
gly1a	0.0074		1			1	
gly1b	0.0074		1			1	
his2a	0.025		1			1	
his2b	0.025		1			1	
ile3a	0.0035		1			1	
ile3b	0.0035		1			1	
gln4a	0.0021		1			1	
gln4b	0.0021		1			1	
ile5a	0.00092		1			1	
ile5b	0.00092		1			1	
pro6							
pro7							
gly8	0.0054		1			1	
leu9a	0.0013		1			1	
leu9b	0.0013		1			1	
thr10a	0.0016	overlap	overlap			1	
thr10b	0.0016					1	
gln11	0.0052						
leu12	0.0014	2.4599e-5	57	-2.0870	3.2709e-6	428	-3.1277
leu13a	0.00052	3.7547e-6	13	-2.5434	8.7867e-7	592	-3.2951
leu13b	0.00052			-2.5434	1.1946e-6	435	-3.1380
gln14a	0.0022	9.9414e-6	221	-2.7865	1.2161e-6	1809	-3.8717
gln14b	0.0022			-2.7865	1.1237e-6	1958	-3.9126
gly15a	0.0091	2.2984e-5	396	-3.0875	1.331e-5	684	-3.3697
gly15b	0.0091			-3.0875	1.3105e-5	694	-3.3772
tyr16a	0.0025	1.4601e-5	171	-2.6541	2.4013e-6	1041	-3.5865
tyr16b	0.0025			-2.6541	2.325e-6	1075	-3.6030
thr17a	0.0029	1.6079e-5	180	-2.6806	1.5346e-6	1890	-3.8943
thr17b	0.0029			-2.6806	1.8024e-6	1609	-3.8112
val18a	0.00098	8.1284e-6	121	-2.4755	1.7741e-6	552	-3.2590
val18b	0.00098			-2.4755	2.1648e-6	453	-3.1570
gln19a	0.0024	1.6853e-5	142	-2.5581	2.448e-6	980	-3.5553
gln19b	0.0024			-2.5581	2.7083e-6	886	-3.5032
val20	0.0011	6.3678e-6	173	-2.6601	1.6289e-6	601	-3.3029
leu21a	0.0006	5.1972e-6	97	-2.3614	1.4454e-6	415	-3.1117
leu21b	0.0006			-2.3614	2.3846e-6	252	-2.8542
arg22	0.0023	1.503e-5	153	-2.5967	2.7461e-6	838	-3.4745
gln23a	0.0059	overlap	overlap		6.5466e-6	901	-3.5119
gln23b	0.0059				6.6893e-6	882	-3.5009
gln24a	0.0056	2.1671e-5	258	-2.8664	1.9844e-5	282	-2.9123
gln24b	0.0056			-2.8664	2.2109e-5	253	-2.8563
pro25							
pro26							
asp27	0.0059		1			1	
leu28	0.0017		1			1	
val29	0.0046		1			1	
asp30	0.0046		1			1	
phe31	0.0036	overlap	overlap		overlap	overlap	
ala32	0.0036	6.7822e-6	531	-3.2390	1.3976e-6	2576	-4.0541
val33a	0.00064	5.8538e-6	109	-2.4216	2.0963e-6	305	-2.9528
val33b	0.00064			-2.4216	2.4887e-6	257	-2.8644
gln34	0.0024	1.3071e-5	184	-2.6919	3.5983e-6	649	-3.3426
tyr35a	0.0029	9.539e-6	304	-2.9511	2.7145e-6	1068	-3.5997
tyr35b	0.0029			-2.9511	2.2135e-6	1310	-3.7051
phe36a	0.002	8.8174e-6	227	-2.8003	1.6674e-6	1199	-3.6594
phe36b	0.002			-2.8003	2.477e-6	807	-3.4550
thr37	0.003	overlap	overlap		overlap	overlap	
arg38	0.0039	1.9527e-5	302	-2.9477	4.6053e-6	1251	-3.6935
leu39	0.0014	1.0874e-5	131	-2.5165	2.2611e-6	619	-3.3181
arg40	0.0023	2.3614e-5	97	-2.3614	1.9991e-5	115	-2.4493
gln41	0.0054	overlap	overlap		overlap	overlap	
ala42	0.0054		1		1.3696e-5	1	
arg43	0.0037		1		1.0215e-5	1	
arg44	0.0031		1		7.954e-6	1	

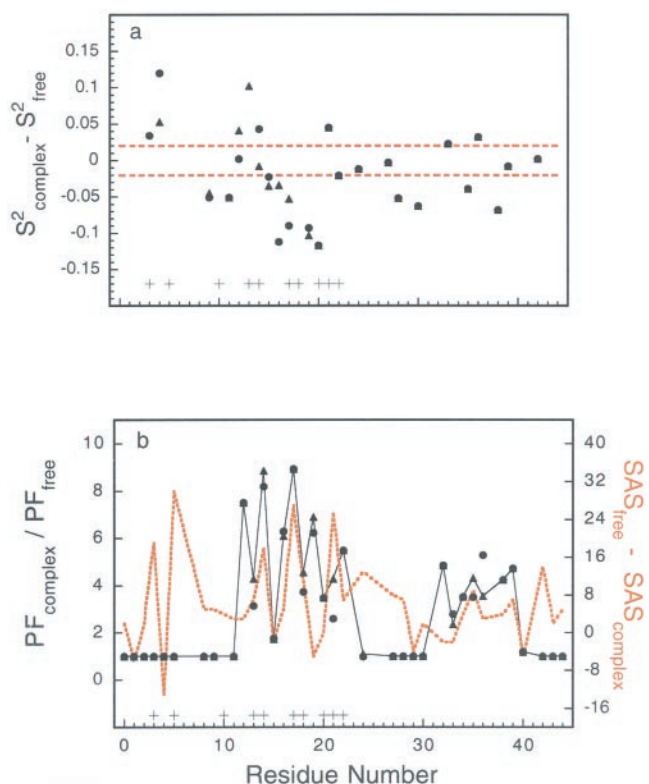


FIG. 1. *a*, differences in order parameters observed between the free and the complexed forms of RII $\alpha$ (1–44). The data between the dashed lines correspond to changes that are not statistically significant (smaller than the root mean square error). Values for promoters A and B are indicated by filled triangles and filled circles, respectively. Contact residues are indicated by a cross in the plot. *b*, differences in the protection factors (solid line) and surface accessible area (red dotted line), observed between the free and the complexed forms of RII $\alpha$ (1–44). Contact residues are indicated by a cross in the plot. The surface accessible area was calculated with MolMol (61).

into deuterated buffer via a QuikChange gel chromatography probe (Roche Molecular Biochemicals). A series of two-dimensional <sup>1</sup>H-<sup>15</sup>N heteronuclear single quantum coherence spectra (17) were collected on a Bruker DMX500 spectrometer at 0, 16, 30, 60, 100, 300, 1080, 1560, and 2880 min after the introduction of the sample into D<sub>2</sub>O buffer. Calibration of the individual spectra to correct for protein concentration differences between samples was achieved by normalizing the data to the intensity of the non-exchanging aliphatic resonance of Val<sup>20</sup> H $\gamma$  2\* in a one-dimensional <sup>1</sup>H spectrum taken directly after the completion of the heteronuclear single quantum coherence experiments.

**Analysis of Kinetic Data**—The time-dependent change in the cross-peak intensity (volume) of each amide proton resonance was found to be exponential. Fitting of each of the observed decay curves to an exponential decay function allowed the extraction of the residue specific experimental exchange rate,  $k_{obs}$ , according to,

$$I = e^{-k_{obs} \times t} \quad (\text{Eq. 1})$$

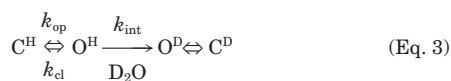
where  $I$  is the observed cross-peak intensity (volume) at time  $t$ . Fitting of data, whether normalized or non-normalized, volume or intensity, from 600 or 500 MHz spectrometer gave identical rates (data not shown).

**Protection Factors**—Residue-specific protection factors,  $P$ , for individual amide protons were calculated from the following relationship,

$$P = k_{int}/k_{obs} \quad (\text{Eq. 2})$$

where  $P$  is the protection factor,  $k_{int}$  the intrinsic rate corrected for local sequence variations (18), and  $k_{obs}$  the observed rate for the solvent exchange of the amide proton.

**Thermodynamic Analysis**—A general form of the hydrogen-deuterium exchange mechanism can be described as (19),



where  $H$  and  $D$  denote protonated and deuterated backbone amides,  $C$  the “closed” form and  $O$  the “open” form, and  $k_{cl}$  and  $k_{op}$  are their corresponding rate constants. The intrinsic rate constant for the chemical exchange reaction,  $k_{int}$ , for a specific amide proton depends upon the local primary sequence, pH, and temperature under which exchange takes place (18, 20). Given this model, the rate constant for the exchange,  $k_{ex}$ , is given by the following relationship.

$$k_{ex} = (k_{op} \times k_{int}) / (k_{cl} + k_{int}) \quad (\text{Eq. 4})$$

When the chemical exchange step is much faster than the rate constant for reprotection, we approach the EX1 limit,  $k_{ex} = k_{op}$ . When the closing step,  $k_{cl}$ , is faster than the exchange rate,  $k_{int}$ , then  $k_{ex}$  reduces to  $k_{ex} = K_{op} \times k_{int}$ , where  $K_{op}$  is the equilibrium constant for the opening reaction. This is known as the EX2 limit. Under these conditions and assuming a well defined native-state ensemble, an apparent free energy of exchange,  $\Delta G_{ex}^{app}$ , can be estimated from the calculated protection factors according to the following relationship,

$$\Delta G_{ex}^{app} = -RT \ln[P] \quad (\text{Eq. 5})$$

where  $R$  is the gas constant,  $T$  the temperature in Kelvin, and  $P$  is the residue-specific protection factor ( $P = k_{ex}/k_{int}$ ) (20).

**NMR Relaxation**—Relaxation experiments were collected at 25 °C on Bruker DMX500 and DRX600 spectrometers using a triple-resonance gradient probe. The <sup>15</sup>N T<sub>1</sub>, <sup>15</sup>N T<sub>2</sub>, and NOE measurements were acquired with established methods that use pulsed-field gradients for coherence transfer pathway selection combined with sensitivity enhancement (21–23). The <sup>15</sup>N T<sub>1</sub> and <sup>15</sup>N T<sub>2</sub> relaxation experiments were collected as a time series of two dimensional <sup>1</sup>H-<sup>15</sup>N correlation spectra, with variable delay times (40, 100\*, 200, 300, 400\*, 500, 600, 800, 100, and 1280 ms for T<sub>1</sub> and 10, 18, 26, 38, 50\*, 62, 78, 98, and 122 ms for T<sub>2</sub>), where asterisks indicate duplicate points to estimate the error in the measured intensities.

TABLE II  
Average values of the  $^{15}\text{N}$  relaxation parameters for the free and complexed RII $\alpha$

Magnetic field		(NOE)	$\langle R_1 \rangle$	$\langle R_2 \rangle$
	MHz		$s^{-1}$	
Free	500	$0.53 \pm 0.06$	$1.83 \pm 0.04$	$8.82 \pm 0.38$
Complex	500	$0.54 \pm 0.06$	$1.69 \pm 0.07$	$9.25 \pm 0.32$
Free	600	$0.59 \pm 0.05$	$1.46 \pm 0.05$	$9.89 \pm 0.49$
Complex	600	$0.67 \pm 0.07$	$1.42 \pm 0.07$	$9.54 \pm 0.35$

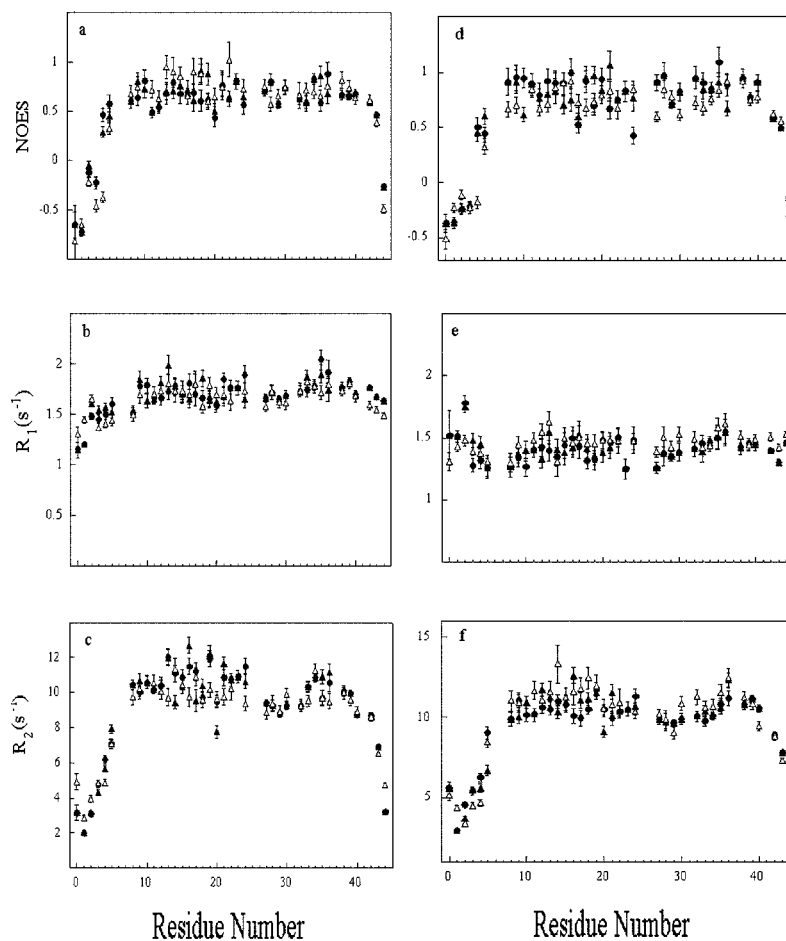


FIG. 2. Plots of the measured  $^{15}\text{N}$  relaxation parameters (heteronuclear NOEs, longitudinal and transverse relaxation rate constants,  $R_1$ , and  $R_2$ , respectively) and their uncertainties as a function of residue number for free (open triangles) and Ht31<sub>pep</sub>-bound RII $\alpha$ (1-44) (filled triangles and circles, corresponding to protomer A and B, respectively). Panels a-c and d-f correspond to data measured at 500 and 600 MHz, respectively.

**Fitting of the Relaxation Data**—Data were processed using the program FELIX 97.0 (Molecular Simulations Inc.) and the intensities for the amide  $^1\text{H}$ - $^{15}\text{N}$  cross-peaks were assessed with *relax\_scripts* (62). The  $R_1$  and  $R_2$  relaxation rates values were determined by fitting the time series to a single exponential decay function. The errors in the rates are reported as the 95% confidence limits in the kinetic fits.  $^1\text{H}$ - $^{15}\text{N}$  steady-state NOE values were determined from the ratio of the intensities of the respective cross-peaks with and without proton saturation. Errors were assessed both from replicate experiments and from measurements of the root mean square values of the noise in the spectra (21).

**Model Free Analysis**—Relaxation of an amide  $^{15}\text{N}$  nucleus is dominated by dipolar coupling with the attached proton, and anisotropy of the  $^{15}\text{N}$  chemical shift tensor. Dynamics of the NH bond axis are characterized by the spectral density function,  $J(\omega)$ , which is related to the three relaxation parameters  $R_1$ ,  $R_2$ , and NOE (24). The model-free formalism (25, 26) allows the assessment of the amplitudes and time scales of the intramolecular motions by modeling the spectral density function,  $J(\omega)$ , in terms of the order parameter  $S^2$  (characterizing the amplitude of internal motions of each NH bond),  $\tau_e$  (the effective correlation time for internal motions), and  $\tau_m$  (the isotropic rotational correlation time of the protein). For an axially symmetric rotational diffusion tensor (27, 28), the spectral density  $J(\omega)$  can be expressed as a function of the angle between the N-H bond vector and the unique axis of the principal frame of the diffusion tensor. We have followed standard protocols (with fitting data acquired at 500 and 600 MHz simulta-

neously) for selection of a dynamical model describing internal motions for each residue (26).

Once the model selection was completed, the parameters characterizing overall molecular tumbling and the internal motional parameters were optimized simultaneously. All optimizations involved minimization of the  $\chi^2$  function (29). The model free calculations were performed using the program *modelfree* (version 4.1), (also *r2r1\_diffusion* and *pdbinertia*) kindly provided by Dr. Arthur G. Palmer. Protomer-specific assignments were used for the D/D in the Ht31<sub>pep</sub> complex except for residues 33, 35, and 36, where it was not possible to obtain unambiguous protomer-specific assignments (10). In the latter cases, Model Free analysis was performed by assigning all possible protomer-specific assignments to resonances (residues 33, 35, and 36). No significant differences were observed in the resulting parameters for residues 33, 35, and 36.

## RESULTS

**Hydrogen/Deuterium Exchange**—Of a total of 44 residues in the RII $\alpha$  D/D protomer, five (Thr<sup>10</sup>, Gln<sup>23</sup>, Phe<sup>31</sup>, Thr<sup>37</sup>, and Glu<sup>41</sup>) in the apo and three (Phe<sup>31</sup>, Thr<sup>37</sup>, and Glu<sup>41</sup>) residues in the Ht31 complex were excluded from analysis because of weak signal intensity and/or resonance overlap. Because the non-palindromic peptide Ht31<sub>pep</sub> binds to RII $\alpha$  in a one peptide to one dimer stoichiometry, it induces asymmetry into the

complex resulting in protomer-specific chemical shift changes in the D/D dimer upon peptide binding (10, 16). Residues on both the exterior and buried faces of helices I/I' and II/II' experience reduction in hydrogen exchange kinetics upon peptide binding (Table I and Fig. 1b). The largest changes in amide exchange rate upon AKAP binding occur in helix I/I' (Leu<sup>12/12'</sup> through Arg<sup>22/22'</sup>), which make up the hydrophobic cleft that is the site of direct AKAP interaction. Mutagenesis studies indicated that residues Ile<sup>3/3'</sup> and Ile<sup>5/5'</sup> contribute important determinants for Ht31<sub>pep</sub> binding (11), but interestingly these residues are freely exchanging in both the apo and the D/D:Ht31<sub>pep</sub> complex. Helices II/II' (Ala<sup>32/32'</sup>-Leu<sup>39/39'</sup>) make up the bottom surface of the molecule and are removed from the AKAP binding surface. Nonetheless, increases in amide-proton exchange protection factors are also observed in this region upon complex formation (Fig. 1b).

**Relaxation**—Backbone <sup>1</sup>H-<sup>15</sup>N resonance assignments of the apo- and Ht31<sub>pep</sub>-bound D/D were determined as described previously (16). Relaxation rate parameters  $R_1$ ,  $R_2$ , and NOE were obtained from the analysis of proton detected <sup>15</sup>N and <sup>1</sup>H correlation spectra of the free and the D/D:Ht31<sub>pep</sub> complex. Data were collected at two magnetic fields, 500 and 600 MHz. 52 of 56 amide proton resonance cross-peaks were of sufficient quality for the reliable quantitation of the cross-peak intensities in the individual spectra. The relaxation parameters are given in Table II. We observe a decrease in the NOE value upon complex formation for most of the residues located in the hydrophobic binding groove, and a concomitant increase in the NOE value for the biologically important residues Ile<sup>3</sup> and Ile<sup>5</sup> (13, 14), among others. These compensatory increases/decreases upon complex formation leads to a system where the domain average NOE values are the same for the free and Ht31<sub>pep</sub> complex, as determined at 500 and 600 MHz (Table II and Fig. 2). Comparison of the  $R_1$  relaxation rates for the apo and Ht31<sub>pep</sub> complex shows a field dependence to the observed domain average rates. The average value for the free is larger than that observed for the complex, when measured at 500 MHz, but is within error as assessed at 600 MHz. The average  $R_2$ , relaxation rates for the free and the complex (at 500 and 600 MHz) are within experimental error, but individual residue rates show variable changes upon complex formation, suggesting the presence of low frequency motions, including possible conformation exchange.

**Model Free Analysis of Relaxation Parameters ( $R_1$ ,  $R_2$ , and NOE)**—We have performed a Model Free analysis (25) of the data in an effort to interpret relaxation parameters in terms of dynamical variables. Chemical shift splitting is observed in the D/D:Ht31<sub>pep</sub> complex and protomer-specific assignments were used where available (see “Experimental Procedures”) (16). The observed residue-specific relaxation parameters (Fig. 2) show an overall (protomer A versus protomer B) similar behavior, thus we included a total of 52 residues in our analysis of the complex.

The experimental data (500 and 600 MHz) were examined assuming either an isotropic or an anisotropic axially symmetric molecular tumbling model. The diffusion tensors of overall reorientation were calculated from the  $R_2/R_1$  ratios (those within one standard deviation of the average (30)) using the program *r2r1\_diffusion* (provided by Dr. Arthur G. Palmer) and the atomic coordinates of the free or Ht31<sub>pep</sub>:D/D complex, respectively (16). The calculated ratio of diffusion tensor components were  $2D_{zz}/(D_{xx} + D_{yy}) = D_{\parallel}/D_{\perp} = 0.97 \pm 0.02$  (free) and  $D_{\parallel}/D_{\perp} = 1.16 \pm 0.02$  (Ht31<sub>pep</sub> complex). Thus, the isotropic model adequately describes the overall reorientation and was used for further analysis.

The overall rotational times,  $\tau_m$ , calculated from  $R_2/R_1$  were

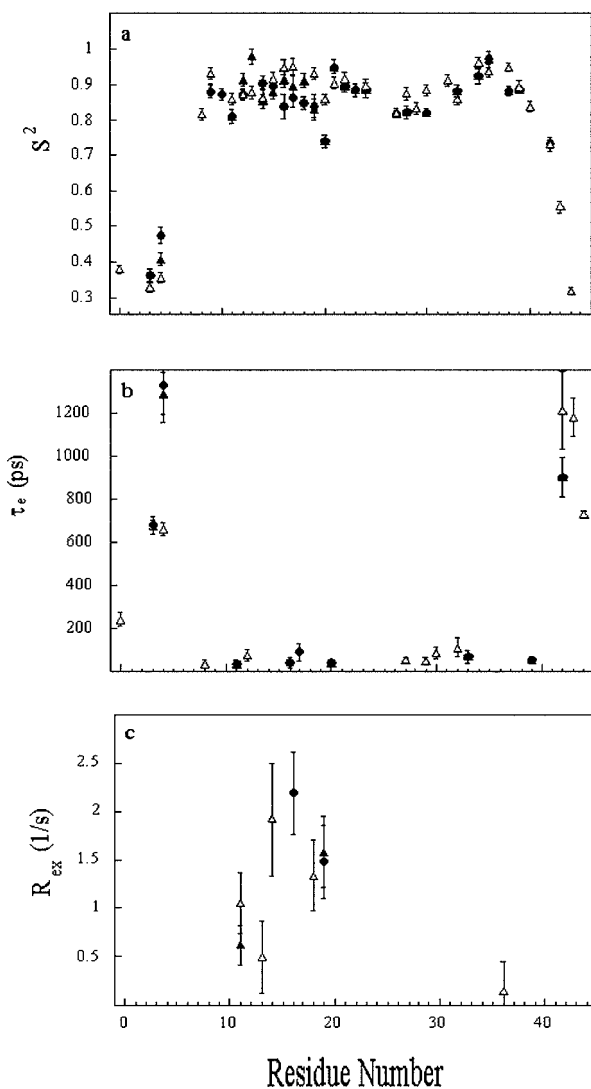


FIG. 3. Plots of optimized Model Free parameters and their uncertainties as a function of residue number for RII $\alpha$ -(1-44) in the free state (open triangles) and in the AKAP bound state (filled triangles and filled circles, corresponding to protomers A and B, respectively). a, the generalized order parameter  $S^2$ ; b, the effective internal correlation time  $\tau_e$ ; c, the exchange broadening contribution  $R_{ex}$ .

used as the initial input values and the final optimization yielded the isotropic correlation times,  $\tau_m$ , of  $7.94 \pm 0.04$  and  $8.25 \pm 0.04$  ns for the free and D/D:Ht31<sub>pep</sub> complex, respectively. A simultaneous fit of the data acquired at 500 and 600 MHz allowed the description of a dynamic model for 36 spins (70% of the total). Residues that could not be fit by a simultaneous protocol are located in the extended and/or disordered regions of the protein. The model free parameters are plotted in Fig. 3, and a table listing these values is supplied (Table III).

#### DISCUSSION

**Structural Overview**—The protomers in the type II $\alpha$  D/D of PKA pack together to form an X-type four-helix bundle with an alternating pattern of (nearly) antiparallel and (nearly) orthogonal helix-helix interactions around the bundle (Fig. 4) (9, 10, 31). The protein core is maintained by strong hydrophobic interactions between side chains that form the dimer interface. In addition, the D/D possesses a hydrophobic groove along the solvent exposed part of the interface of helices I, I' (14). The hydrophobic side chains of this groove cluster against each other and are well defined in the solution structure, despite being solvent

TABLE III  
 Backbone dynamical parameters for the free and complexed RII $\alpha$ 

Residue	S <sup>2</sup> _free	S <sup>2</sup> _complex	S <sup>2</sup> c-S <sup>2</sup> f	$\tau_c$ (ps)_f	$\tau_c$ (ps)_c	R <sub>ex</sub> (s <sup>-1</sup> )_f	R <sub>ex</sub> (s <sup>-1</sup> )_c
Met <sup>0</sup>	0.377 ± 0.012	No model		242 ± 32			
Gly <sup>1</sup>	No model	No model					
His <sup>2a</sup>	No model	No model					
His <sup>2b</sup>	No model	No model					
Ile <sup>3a</sup>	0.327 ± 0.015	No model		672 ± 30			
Ile <sup>3b</sup>	0.327 ± 0.015	0.361 ± 0.016	0.034	672 ± 30	679 ± 39		
Gln <sup>4a</sup>	0.354 ± 0.024	0.407 ± 0.018	0.053	663 ± 30	1290 ± 97		
Gln <sup>4b</sup>	0.354 ± 0.024	0.474 ± 0.024	0.120	663 ± 30	1332 ± 172		
Ile <sup>5a</sup>	No model	No model					
Ile <sup>5b</sup>	No model	No model					
Gly <sup>8</sup>	0.817 ± 0.017	No model		35 ± 18			
Leu <sup>9a</sup>	0.930 ± 0.018	0.885 ± 0.018	-0.045				
Leu <sup>9b</sup>	0.930 ± 0.018	0.879 ± 0.019	-0.051				
Thr <sup>10a</sup>	Overlap	No model					
Thr <sup>10b</sup>	Overlap	0.870 ± 0.017					
Glu <sup>11</sup>	0.859 ± 0.017	0.808 ± 0.021	-0.051		37 ± 13	1.057 ± 0.3	0.6 ± 0.2
Leu <sup>12a</sup>	0.871 ± 0.016	0.912 ± 0.017	0.041	76 ± 27			
Leu <sup>12b</sup>	0.870 ± 0.016	0.873 ± 0.017	0.003	75 ± 26			
Leu <sup>13a</sup>	0.877 ± 0.020	0.979 ± 0.022	0.102			0.498 ± 0.3	
Leu <sup>13b</sup>	0.877 ± 0.020	No model				0.498 ± 0.3	
Gln <sup>14a</sup>	0.861 ± 0.027	0.853 ± 0.019	-0.008			1.918 ± 0.58	
Gln <sup>14b</sup>	0.861 ± 0.027	0.904 ± 0.020	0.043			1.918 ± 0.58	
Gly <sup>15a</sup>	0.915 ± 0.019	0.880 ± 0.021	-0.035				
Gly <sup>15b</sup>	0.915 ± 0.019	0.895 ± 0.022	-0.020				
Tyr <sup>16a</sup>	0.948 ± 0.022	0.836 ± 0.035	-0.11		40 ± 23		2.1 ± 0.4
Tyr <sup>16b</sup>	0.948 ± 0.022	0.914 ± 0.022	-0.034				
Thr <sup>17a</sup>	0.950 ± 0.022	0.897 ± 0.025	-0.053				
Thr <sup>17b</sup>	0.950 ± 0.022	0.860 ± 0.024	-0.090		90 ± 44		
Val <sup>18a</sup>	No model	0.910 ± 0.019					
Val <sup>18b</sup>	No model	0.846 ± 0.017					
Glu <sup>19a</sup>	0.931 ± 0.018	0.838 ± 0.032	-0.093				1.4 ± 0.3
Glu <sup>19b</sup>	0.931 ± 0.018	0.828 ± 0.030	-0.103				1.5 ± 0.3
Val <sup>20</sup>	0.857 ± 0.015	0.740 ± 0.017	-0.117		38 ± 13		
Leu <sup>21</sup>	0.904 ± 0.016	0.949 ± 0.020	0.045				
Arg <sup>22</sup>	0.915 ± 0.019	0.894 ± 0.017	-0.021			0.154 ± 0.1	
Gln <sup>23</sup>	Overlap	0.884 ± 0.018					
Gln <sup>24</sup>	0.896 ± 0.016	0.884 ± 0.022	-0.012				
Asp <sup>27</sup>	0.819 ± 0.015	0.816 ± 0.010	-0.003	52 ± 13			
Leu <sup>28</sup>	0.874 ± 0.019	0.822 ± 0.019	-0.052				
Val <sup>29</sup>	0.832 ± 0.015	No model		45 ± 18	32 ± 11		
Asp <sup>30</sup>	0.884 ± 0.016	0.821 ± 0.013	-0.063	85 ± 29			
Ala <sup>32</sup>	0.912 ± 0.015	No model		111 ± 43			
Val <sup>33</sup>	0.858 ± 0.014	0.881 ± 0.017	0.023		67 ± 31		
Glu <sup>34</sup>	No model	No model					
Tyr <sup>35</sup>	0.961 ± 0.014	0.922 ± 0.021	-0.039				
Phe <sup>36</sup>	0.939 ± 0.019	0.971 ± 0.023	0.032			0.61 ± 0.7	0.75 ± 0.80
Arg <sup>38</sup>	0.949 ± 0.012	0.881 ± 0.013	-0.068				
Leu <sup>39</sup>	0.893 ± 0.015	0.885 ± 0.010	-0.008		53 ± 18		
Arg <sup>40</sup>	0.836 ± 0.014	No model					
Ala <sup>42</sup>	0.731 ± 0.020	0.733 ± 0.010	0.002	1271 ± 180	903 ± 92		
Arg <sup>43</sup>	0.554 ± 0.015	No model		1184 ± 92			
Arg <sup>44</sup>	0.315 ± 0.010	No model		732 ± 15			

exposed. This is an unusual, but significant characteristic of the D/D, which promotes participation in protein-protein interactions with a diverse family of anchoring proteins (32).

Mapping studies on a growing family of anchoring proteins have helped define a primary sequence of 20 amino acids that exhibit a high probability of amphipathic helix formation that is the likely site for D/D binding (33). Ht31<sub>pep</sub> has emerged as the prototypic AKAP and structural studies confirmed the role of hydrophobic groups from the amphipathic helix of Ht31 for high-affinity D/D anchoring interactions (11). Indeed Ht31<sub>pep</sub> is a powerful reagent for the disruption of PKA anchoring inside cells (11). As Ht31<sub>pep</sub> displaces a wide variety of AKAP partners *in vivo*, it emerges as the ideal system for understanding AKAP recognition by PKA (14, 32).

**Hydrogen Exchange in the Ht31<sub>pep</sub>·D/D Complex**—In principle, the changes in the amide-exchange protection factors of the slowest exchanging protons upon ligand binding can be used to extract thermodynamic binding constants, given that the protein is undergoing amide exchange in the EX(2) limit (see “Experimental Procedures”) (15, 34). EX(2) is generally the

dominating exchange mechanism for backbone amide protons in proteins under conditions where the native state is stable and the intrinsic exchange rate is slow. A pH rate study to test for the possibility of EX(1) exchange in the D/D was not possible due the fact that the protein tends to aggregate under pH conditions different from 4.0 (16). However, mass spectrometric analysis of the exchange upon peptide binding showed no evidence for EX(1) exchange.<sup>2</sup> Thus, we initially interpreted our results assuming an EX(2) model.

Unlike the observation of Powell *et al.* (15) where the observed changes in amide proton exchange rates are in good agreement with those predicted from the measured ligand binding affinities, we have found that the calculation of the thermodynamic binding constant from the observed changes in protection factors greatly underestimates the Ht31<sub>pep</sub> binding affinity (Table I and Fig. 1b). Instead, our data suggests that the D/D exchanges either through local breathing motions (35)

<sup>2</sup> L. Burns, unpublished results.

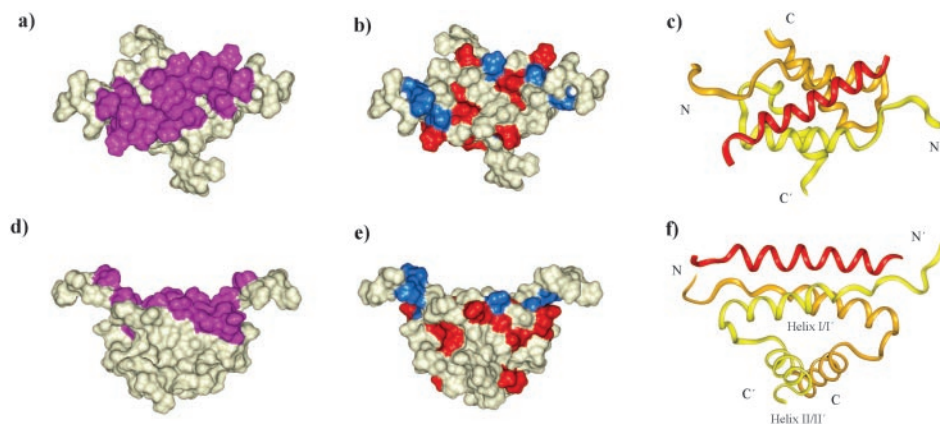


FIG. 4. **Color coding of the observed changes in backbone dynamics of RII $\alpha$  D/D upon Ht31<sub>pep</sub> binding.** Different views of the dimer. *a*, Connolly surface representation of bound RII $\alpha$ (1–44). Residues colored in *magenta* make contact to the AKAP. *b*, color coding of changes in order parameter with the same orientation view as in *a*. Residues that showed changes in order parameter ( $\Delta S^2 = S_{\text{com}}^2 - S_{\text{apo}}^2$ ) upon binding are colored as *red*,  $\Delta S^2 < 0$ , and *blue*,  $\Delta S^2 > 0$ . Residues that did not show significant change upon binding or for which data are not available are shown in *gray*. *c*, ribbon diagram of the RII $\alpha$ (1–44)-Ht31<sub>pep</sub> complex. The RII $\alpha$ (1–44) protomers are colored in *orange* and *yellow*, whereas the AKAP peptide is in *red*. *d–f* are as *a*, *b*, and *c*, respectively, but with different views.

or behaves as a highly dynamic conformational ensemble composed of nearly isoenergetic states, which differ slightly in their exchange properties (36). In the latter case, binding energy is used for the redistribution of the ensemble without the necessity of restricting the backbone motions that allow for H/D exchange (37). Interestingly, members of the calmodulin family and protein L9, which also bind a diverse family of targets, show minimal exchange protection upon target binding (38, 39).

**The Distribution of Order Parameters**—Whereas the values of  $S^2$  for the *entire* D/D domain in the free and Ht31-bound RII $\alpha$  (Fig. 3*a*) are within error, there are differences observed between the two species when compared at the residue level (Fig. 1*a*). Interestingly, both *increases* (10 residues) and *decreases* (21 residues) in order parameter were observed upon complex formation (Fig. 4, *b* and *e*). Many residues in the hydrophobic peptide-binding groove (Fig. 4*b*) showed decreases ( $\Delta S^2 < 0$ ) in order parameter, indicating that the residues within this binding cleft are *more flexible* in the Ht31<sub>pep</sub>-D/D complex. These changes are mapped onto the structure in Fig. 4, *b* and *e*, and include Leu<sup>9</sup>, Glu<sup>11</sup>, Gly<sup>15</sup> (only protomer A), Tyr<sup>16</sup>, Thr<sup>17</sup>, Glu<sup>19</sup>, Val<sup>20</sup> (which demonstrates a very large decrease), and Arg<sup>22</sup>. Other residues with decreases in the observed order parameter are Leu<sup>28</sup>, Asp<sup>30</sup>, and Arg<sup>38</sup>. Increases in order parameter are observed (reflecting *restricted* motions) in residues Ile<sup>3</sup> (only protomer B), Gln<sup>4</sup> (both located in the extended N terminus region), Leu<sup>12</sup> (only protomer A), Leu<sup>13</sup> (only protomer A), Gln<sup>14</sup> (only protomer B), Leu<sup>21</sup> (in the first helix), and Phe<sup>36</sup> (in the second helix).

**Internal Motion  $\tau_e$  and Exchange Broadening Factor  $R_{ex}$** —Most residues in helix I and II are well characterized by the original Lipari-Szabo (25) formalism in which the internal motions are described by the order parameter and the effective internal correlation time,  $\tau_e$ . Residues that are disordered in the NMR structures (including the first five residues in the N terminus and the last six of the C terminus) were better described with three parameters ( $S_s^2$ ,  $S_f$ , and  $\tau_e$ ) for slow and fast internal modes (see Fig. 3*b* and Table III). Inclusion of an exchange-broadening factor (Table III and Fig. 3*c*) to account for  $\mu$ s-ms motions was necessary for a few residues located in the first helix (Glu<sup>11</sup>, Leu<sup>13</sup>, Gln<sup>14</sup>, and Arg<sup>22</sup> for the free D/D and Glu<sup>11</sup>, Tyr<sup>16</sup>, and Glu<sup>19</sup> for the complex), and for one residue, Phe<sup>36</sup>, located in the second helix in both forms. This region encompasses the hydrophobic binding groove, and may reflect conformational exchange processes, consistent with the

ensemble view of protein dynamics (40). A similar effect was also observed in studies on the C-terminal domain of *Escherichia coli* topoisomerase I bound to a single-stranded DNA (41).

**Conformational Entropy Changes Because of Complex Formation**—Protein-protein interactions control a diverse set of biological functions, yet we still do not have a full understanding of target recognition. Clearly, the molecular basis for protein target binding is controlled by a variety of factors including favorable binding enthalpy as well as changes in solvent, side chain, and backbone entropies of the interacting partners (42, 43). As we observed unexpected *increases* in backbone motions as a result of complex formation, we were interested in estimating the contribution of these motions to the overall Gibbs free energy of binding. The energetic benefit associated with increases in backbone flexibility upon binding can be estimated from the experimental relaxation data, using the experimentally measured order parameters,  $S^2$  (44, 45). This model assumes that the bond motions of all NH vectors are independent and provides an upper limit to the true value, as the model is simplified with the assumption of complete independence of motions (44). Nonetheless, the correlation between observed changes in order parameters (and the derived entropy values) and ligand binding/activity supports the examination of these parameters (46, 47). The entropic contribution to the free energy of binding,  $\Delta G$ , was determined as described previously (44),

$$\Delta G = G_{\text{complex}} - G_{\text{free}} = -RT \sum \ln[(1 - S_{\text{complex}}^2)/(1 - S_{\text{free}}^2)] \quad (\text{Eq. 6})$$

where  $S^2$  is the order parameter,  $R$  is the molar gas constant, and  $G$  is the free energy of Gibbs. Complex formation leads to a small, but favorable, entropic contribution to the Gibbs free energy of binding ( $\Delta G = \Delta H - T\Delta S$ ) at  $T = 25^\circ\text{C}$  of  $-T\Delta S = -3.7 \pm 1$  kcal/mol. The total binding free energy change calculated from the dissociation constant ( $K_D = 16$  nM) for the Ht31<sub>pep</sub>-RII $\alpha$  interaction (16) yields a value of  $-10.53$  kcal/mol. The corresponding value calculated (see “Experimental Procedures”) from the changes in protection factors of the core residues upon binding is  $\Delta G = -0.62$  kcal/mol, which is much smaller than calculated from the dissociation constant, and may be explained with the idea of the protein being a highly dynamic collection of states (37).

**Adaptive Sites in Protein Target Recognition**—In the majority of studies on the backbone and/or side chain dynamics of

molecular complexes, decreased motions upon complex formation are observed, as is expected from an "induced-fit" mechanism (48–50). In these cases, binding is associated with a loss of conformational entropy that is necessarily offset by increases in solvent entropy and/or the formation of favorable enthalpic interactions. Decreases/increases in backbone dynamics that are compensated for by increases/decreases (respectively) in distal regions in the backbone, as we report here, have also been found for protein hydrophobic target interactions (21, 41, 45, 51–55). It may be that the observed increase in flexibility in the binding pocket accompanies the release of structured water molecules from the solvent accessible hydrophobic surfaces. This solvent release could induce a concurrent disordering of the protein structure (52, 56) and remains an area of significant interest. Interestingly, in all cases of increased dynamics upon binding, reported to date, occur in proteins that recognize diverse targets through hydrophobic interactions. Thus, a reasonable hypothesis would be that these proteins use this increased plasticity (either in backbone and/or side chain domain) to accommodate the differences between target molecules.

Interestingly, structural analysis of various complexes of bacterial phosphotransferase pathway, involving the protein HPr (57, 58), shows that this protein can interact with proteins of drastically different folds (e.g. EI, IIAGlucose, IIAMannitol) yet uses the same recognition surface (58). Relaxation studies on Crh, a structural homolog of Hpr, indicate that it also experiences increased flexibility upon target binding (59). Whereas side chain plasticity is obviously important in protein/protein recognition in the HPr system (58), it would be interesting to determine whether the relaxation properties for the Hpr complexes described above were consistent with its structural homolog and was a characteristic of proteins that interact with many partners. Like the RII $\alpha$  D/D, the consensus binding site on HPr is an adaptive, highly exposed and energetically important region that is primed for interaction with diverse molecules (58). However, in the case of the RII $\alpha$  D/D, although the sequences of AKAPs are diverse, until recently the structural motifs in recognition appeared to be conserved (14). Recent evidence indicates that the centrosomal anchoring protein, pericentrin, appears to present a novel interaction motif for the D/D (60). Further structural studies of this anchoring partner will highlight the range of structural motifs capable of participating in anchoring interactions. Clearly, conservation of hydrophobicity will remain an important recognition mechanism for tethering PKA through its D/D to diverse anchoring partners.

**Acknowledgments**—We gratefully acknowledge Drs. David Heidary and Melinda Roy for critical reading of the manuscript, Dr. Larry Gross for mass spectrometric analysis, Dr. Dimitrios Morikis for software to calculate the intrinsic exchange rates, and the Keck Institute for computational support.

## REFERENCES

- Wells, J. A., and de Vos, A. M. (1996) *Annu. Rev. Biochem.* **65**, 609–634
- Pawson, T., and Scott, J. D. (1997) *Science* **278**, 2075–2080
- Hunter, T. (2000) *Cell* **100**, 113–127
- Lester, L. B., and Scott, J. D. (1997) *Recent Prog. Horm. Res.* **52**, 409–429
- Colledge, M., and Scott, J. D. (1999) *Trends Cell Biol.* **9**, 216–221
- Taylor, S. S., Buechler, J. A., and Yonemoto, W. (1990) *Annu. Rev. Biochem.* **59**, 971–1005
- Hausken, Z. E., Coghlan, V. M., Hastings, C. A., Reimann, E. M., and Scott, J. D. (1994) *J. Biol. Chem.* **269**, 24245–24251
- Hausken, Z. E., Dell'Acqua, M. L., Coghlan, V. M., and Scott, J. D. (1996) *J. Biol. Chem.* **271**, 29016–29022
- Newlon, M. G., Roy, M., Morikis, D., Hausken, Z. E., Coghlan, V., Scott, J. D., and Jennings, P. A. (1999) *Nat. Struct. Biol.* **6**, 222–227
- Newlon, M. G., Roy, M., Morikis, D., Carr, D. W., Westphal, R., Scott, J. D., and Jennings, P. A. (2001) *EMBO J.* **20**, 1651–1662
- Carr, D. W., Hausken, Z. E., Fraser, I. D., Stofko-Hahn, R. E., and Scott, J. D. (1992) *J. Biol. Chem.* **267**, 13376–13382
- Carr, D. W., Stofko-Hahn, R. E., Fraser, I. D., Cone, R. D., and Scott, J. D. (1992) *J. Biol. Chem.* **267**, 16816–16823
- Vijayaraghavan, S., Liberty, G. A., Mohan, J., Winfrey, V. P., Olson, G. E., and Carr, D. W. (1999) *Mol. Endocrinol.* **13**, 705–717
- Carr, D. W., Stofko-Hahn, R. E., Fraser, I. D., Bishop, S. M., Acott, T. S., Brennan, R. G., and Scott, J. D. (1991) *J. Biol. Chem.* **266**, 14188–14192
- Powell, K. D., Ghaemmaghami, S., Wang, M. Z., Ma, L., Oas, T. G., and Fitzgerald, M. C. (2002) *J. Am. Chem. Soc.* **124**, 10256–10257
- Newlon, M. G., Roy, M., Hausken, Z. E., Scott, J. D., and Jennings, P. A. (1997) *J. Biol. Chem.* **272**, 23637–23644
- Mori, S., Abeygunawardana, C., Johnson, M. O., and van Zijl, P. C. (1995) *J. Magn. Reson. B* **108**, 94–98
- Bai, Y., Milne, J. S., Mayne, L., and Englander, S. W. (1993) *Proteins* **17**, 75–86
- Hvidt, A. A., and Nielsen, S. O. (1966) *Adv. Protein Chem.* **21**, 287–386
- Molday, R. S., Englander, S. W., and Kallen, R. G. (1972) *Biochemistry* **11**, 150–158
- Farrow, N. A., Muhandiram, R., Singer, A. U., Pascal, S. M., Kay, C. M., Gish, G., Shoelson, S. E., Pawson, T., Forman-Kay, J. D., and Kay, L. E. (1994) *Biochemistry* **33**, 5984–6003
- Kay, L. E., Nicholson, L. K., Delaglio, F., Bax, A., and Torchia, D. A. (1992) *J. Magn. Reson.* **97**, 359–375
- Markley, J. L., Horsley, W. J., and Klein, M. P. (1971) *J. Chem. Phys.* **55**, 3604–3611
- Abragam, A. (1961) *Principles of Nuclear Magnetism*, Clarendon Press, Oxford
- Lipari, G., and Szabo, A. (1982) *J. Am. Chem. Soc.* **104**, 4546–4570
- Clare, G. M., Driscoll, P. C., Wingfield, P. T., and Gronenborn, A. M. (1990) *Biochemistry* **29**, 7387–7401
- Schurr, J. M., Babcock, H. P., and Fujimoto, B. S. (1994) *J. Magn. Reson. B* **105**, 211–224
- Tjandra, N., Feller, S. E., Pastor, R. W., and Bax, A. (1995) *J. Am. Chem. Soc.* **117**, 12562–12566
- Mandel, A. M., Akke, M., and Palmer, A. G., 3rd (1995) *J. Mol. Biol.* **246**, 144–163
- Kay, L. E., Torchia, D. A., and Bax, A. (1989) *Biochemistry* **28**, 8972–8979
- Harris, N. L., Presnell, S. R., and Cohen, F. E. (1994) *J. Mol. Biol.* **236**, 1356–1368
- Scott, J. D., and McCartney, S. (1994) *Mol. Endocrinol.* **8**, 5–11
- Alto, M. N., Soderling, S. H., Hoshi, N., Langeberg, L. K., Fayos, R., Jennings, P. A., and Scott, J. D. (2003) *Proc. Natl. Acad. Sci. U.S.A.*, in press
- Ghaemmaghami, S., Fitzgerald, M. C., and Oas, T. G. (2000) *Proc. Natl. Acad. Sci. U.S.A.* **97**, 8296–8301
- Clarke, J., Hounslow, A. M., Bycroft, M., and Fersht, A. R. (1993) *Proc. Natl. Acad. Sci. U.S.A.* **90**, 9837–9841
- Baxter, N. J., Hosszu, L. L., Waltho, J. P., and Williamson, M. P. (1998) *J. Mol. Biol.* **284**, 1625–1639
- Hong Pan, J. C. L., and Hilsner, V. J. (2000) *Proc. Natl. Acad. Sci. U. S. A.* **97**, 12020–12025
- Lillemoen, J., Cameron, C. S., and Hoffman, D. W. (1997) *J. Mol. Biol.* **268**, 482–493
- Ohki, S., Tsuda, S., Joko, S., Yazawa, M., Yagi, K., and Hikichi, K. (1991) *J. Biochem. (Tokyo)* **109**, 234–237
- Hilsner, V. J., Dowdy, D., Oas, T. G., and Freire, E. (1998) *Proc. Natl. Acad. Sci. U. S. A.* **95**, 9903–9908
- Yu, L., Zhu, C., Tse-Dinh, Y., and Fesik, S. W. (1996) *Biochemistry* **35**, 9661–9666
- Forman-Kay, J. D. (1999) *Nat. Struct. Biol.* **6**, 1086–1087
- Cavanagh, J., and Akke, M. (2000) *Nat. Struct. Biol.* **7**, 11–13
- Akke, M., Skelton, N. J., Kordel, J., Palmer, A. G., 3rd, and Chazin, W. J. (1993) *Biochemistry* **32**, 9832–9844
- Stivers, J. T., Abeygunawardana, C., and Mildvan, A. S. (1996) *Biochemistry* **35**, 16036–16047
- Fischer, M. W., Majumdar, A., and Zuiderweg, E. R. (1998) *Prog. Nuclear Mag. Res. Spectr.* **33**, 207–272
- Lu, J., Lin, C. L., Tang, C., Ponder, J. W., Kao, J. L., Cistola, D. P., and Li, E. (1999) *J. Mol. Biol.* **286**, 1179–1195
- Dyson, H. J., and Wright, P. E. (2001) *Methods Enzymol.* **339**, 258–270
- Osborne, M. J., Schnell, J., Benkovic, S. J., Dyson, H. J., and Wright, P. E. (2001) *Biochemistry* **40**, 9846–9859
- Krishnan, V. V., Sukumar, M., Gierasch, L. M., and Cosman, M. (2000) *Biochemistry* **39**, 9119–9129
- Li, F., Gangal, M., Juliano, C., Gorfain, E., Taylor, S. S., and Johnson, D. A. (2002) *J. Mol. Biol.* **315**, 459–469
- Zidek, L., Novotny, M. V., and Stone, M. J. (1999) *Nat. Struct. Biol.* **6**, 1118–1121
- Glover, K. J., Whiles, J. A., Wood, M. J., Melacini, G., Komives, E. A., and Vold, R. R. (2001) *Biochemistry* **40**, 13137–13142
- Huster, D., and Gawrisch, K. (1999) *J. Am. Chem. Soc.* **121**, 1992–1993
- Yun, S. G., Jang, D. S., Kim, D. H., Choi, K. Y., and Lee, H. C. (2001) *Biochemistry* **40**, 3967–3973
- Morton, A., and Matthews, B. W. (1995) *Biochemistry* **34**, 8576–8588
- Herzberg, O., and Kleit, R. (1994) *Curr. Opin. Struct. Biol.* **4**, 814–822
- Wang, G., Sondej, M., Garrett, D. S., Peterkofsky, A., and Clare, G. M. (2000) *J. Biol. Chem.* **275**, 16401–16403
- Favier, A., Brutscher, B., Blackledge, M., Galinier, A., Deutscher, J., Penin, F., and Marion, D. (2002) *J. Mol. Biol.* **317**, 131–144
- Diviani, D., Langeberg, L. K., Doxsey, S. J., and Scott, J. D. (2000) *Curr. Biol.* **10**, 417–420
- Koradi, R., Billeter, M., and Wuthrich, K. (1996) *J. Mol. Graph.* **14**, 29–32, 51–55
- Akke, M. (1994) *relax\_scripts*, Lund University, Lund, Sweden